SAND2021-11314C

Steady & Transient Heating & Cooling Analysis for High-Temperature Chloride Molten Salt Storage Tanks

Kenneth Armijo[1, a)], Nicolas Delovato[1)] and Aaron Overacker[1)]

[1] Concentrating Solar Technology, Sandia National Laboratories, P.O. Box 5800, MS-1127, Albuquerque, NM 87185, USA
[a)] kmarmij@sandia.gov

Abstract. A Generation 3 Liquid-Pathway project Chloride salt tank system was designed for pilot-scale 1 MWth testing at the National Solar Thermal Test Facility (NSTTF) in Albuquerque, NM, USA. This prototype Gen 3, concentrating solar power (CSP) system was designed to facilitate a minimum of 6 hrs. of thermal energy storage (TES) with operational nominal temperatures of 500 °C and 720 °C for a cold and hot tank respectively. For this investigation, the researchers developed two steady and transient computational fluid mechanics (CFD) circulation models to assess thermal-fluid behavior within the tanks, and their respective interactions with environmental heat transfer. The models developed for this novel CSP system design will include unique chloride molten salt thermodynamic properties and correlations. The results of this investigation suggest thermal gradients for the steady flow model less 1°C with overall circulation velocities as high as approximately 2.1 m/s. Higher steady flow rates of salt passing into and out of the tanks resulted in smaller thermal gradients than the slower flow rates as the molten salt mixes better (an increase of around 120% in the heat transfer coefficient) at the higher velocities associated with the higher flow rate. The port spacing of 3.85 m was found to have a highly uniform temperature distribution. For the unsteady model, nitrogen flow was found to become steady after approximately 10 minutes and the molten salt flow was found to increase slowly as the overall molten salt level rose.

INTRODUCTION

For current, state-of-the-art CSP power tower TES technologies, two-tank systems using molten salt as the heat transfer fluid (HTF), is the most used configuration. Advantages of this sensible TES technology approach allow for reliable circulation using a pump as well as bulk thermal fluid control within the tanks under varying operational modes (i.e. charging and discharging). This is in contrast to other (PCM, solid media, etc.), where design aspects which have a number of thermal transport issues [1], however thermal management challenges still exist such as controlling the thermal losses, possible freezing and optimization of the storage (aspect ratio, design of the inlet ports, etc.). The design and optimization thermal storage tanks require operational knowledge of the thermal and fluid hydraulics physical phenomena involved, particularly with regards to both natural and forced convection. Due to the complexity of internal TES tank topologies, with a number of pumps, level and possible chemistry sensors, etc. phenomena associated with internal thermal-fluid behavior with regard to their theoretical optimized thermal transport design is a challenge for researchers and engineers developing large tanks for long duration storage, particularly beyond 10 hrs. Gen 3 targets [2]. A Generation 3 Liquid-Pathway project Chloride salt tank system was designed for pilot-scale 1 MW_{th} testing at the National Solar Thermal Test Facility (NSTTF) in Albuquerque, NM, USA. This prototype system was designed to facilitate a minimum of 6 hrs. of thermal energy storage (TES) with operational nominal temperatures of 500°C and 720 °C for a cold and hot tank respectively. To characterize the multimode heat transfer behavior within a CSP TES system, numerous studies have made the assumptions of near-isothermal behavior [3] based on relatively large volumes of salt present within either a cold or hot tank [4]. However, within each salt tank both natural circulation as well as forced convection contribute to heating profiles that can impact the temperatures of the salt that leaves the tanks, either to flow to the receiver (cold tank), or to discharge to a power block heat exchanger (hot tank). To date few papers have assessed both natural and forced convection of molten salt within TES systems, particularly under transient conditions, and for TES target temperatures above 600°C. Several computational fluid dynamics or other global models have been developed; however, many consider only low-temperature applications [5-8]. For example, Gabbrielli and Zamparelli [9] presented a global storage models for selecting optimal numerical parameters for molten salt tanks, though for temperatures up to 550°C. For low temperature applications, Papanicolaou and Belessiotis [10] investigated transient natural convection inside a vertical cylinder with an imposed heat flux, which considered Reynolds averaged Navier–Stokes (RANS) equations with different turbulent models to improve accuracy of more realistic behavior. However, challenges with the lack of empirical information about internal tank heat transfer coefficients, particularly in thermal commercial storage tanks, or HTF temperatures >550°C have not been available, therefore CFD models have mostly been used to obtain

correlations capable of readily characterizing both steady and transient heat transfer process inside TES molten salt tanks [11,12]. However, as Rodríguez et al. noted [1], many computational correlations developed are in the range of Rayleigh numbers corresponding with low-temperature CSP (particularly <400°C), and not particularly suited for molten salt TES. Among different storage systems investigated for high temperature applications, thermocline storage systems have received much attention within computational studies for multi-dimensional simulations (mostly two-dimensional) [13,14]. Some studies, such as Gandhi et al. [15], assessed flow patterns and temperature in centrally heated cylindrical tanks while investigating the effect internal structures like fins and draft tubes on stratification and flow. Their simulation results showed reasonable agreement between predicted and experimental results pertaining to heat transfer coefficients within the tank for unsteady operation. However, less consideration has been applied to two-molten salt systems with temperatures >585°C. Within molten salt TES, heat transfer and fluid flow phenomena can present very complex thermal-fluid phenomena when it pertains to mixing, flow around structures, as well as radiative heat exchange between free surfaces of the salt and the tank walls, turbulent convections at very high Rayleigh numbers of the molten salt in the tank, heat losses from the multi-layered tank foundations, among others [1]. This thermal-fluids interplay can present significant challenges for accurately simulating such systems, particularly with HTF temperatures that are significantly higher, which can also impact the thermal-mechanical integrity of the tank materials as well. For this investigation, a steady and transient computational fluid mechanics (CFD) circulation models are developed to assess thermal-fluid behavior within the tanks, and their respective interactions with environmental heat transfer. This novel analysis also evaluated resultant temperature impacts at the inlet and outlet ports within the tanks, which can impact thermal performance within the rest of a simulated molten salt system [16]. The models developed for this novel design include a unique ternary chloride (20%NaCl/40%$MgCl_2$/40%KCl by mol wt.%) molten salt chemistry thermodynamic properties and correlations. This work considers thermal-fluid interactions within a cold and hot tank with target bulk temperatures of approximately 500°C and 720°C respectively. These models also consider the impact of thermal-fluid transport with respect to tank inlet and outlet piping and the impacts of heat transfer and operation for a Gen 3 2.0 MW_{th} pilot-scale system.

NUMERICAL DEVELOPMENT

Circulating Flow Model

Modeling for the operation of the molten salt tanks was developed using ANSYS Fluent software and involved a coupled computational fluid dynamics (CFD) and thermal finite element analysis (FEA). Flow, turbulence, and energy constitutive equations were solved for all operational phases of the two Gen 3 molten salt tanks. The scale of molten salt tanks and the modeled physics required a large amount of computational resources demand, therefore the use of reduced ordered models improved model processor efficiency. Two dimensional models were used in the simulations of the circulating flow, charging, and discharging operational modes. **Error! Reference source not found.** shows the two-dimensional geometry used within the simulation modelling domain that was used to characterize the circulation flow phase. Molten salt is simulated to enter the tank at label A and exit at label B. The design of salt piping inlet and outlet ports was altered from the tank's true design due to the two-dimensional nature of the model. Modeling the tanks in two dimensions with flow pipes which transverse the height of the tanks would restrict flow in the tank. This flow restriction would in turn be unrealistic as the molten salt within the tank would be easily by able flow around the inlet and outlet piping. To better represent 3D flow in two dimensions, two small, 1 cm, portions of the piping were created in the model to flow the molten salt in and out of the tank. These small portions of the piping contain either an inlet or outlet the size of the inner diameter of the pipe surrounded by wall-type boundary conditions (BCs) the size of the wall thickness of the pipe. These wall-type BCs surrounding the inlet and outlet were needed for convergence of the flow. The small portions of the piping allowed for flow more freely travel around the tank and to be more representative of the flow in the actual tank. The density of the nitrogen was approximated with the Boussinesq model, Eqn. 1. ***Error! Reference source not found.***The Boussinesq model was used based on steady-state calculations of the nitrogen as buoyancy-driven flow inside of a closed domain for convergence stability.

$$(\rho - \rho_0)g \approx -\rho_0\beta(T - T_0)g \quad (1)$$

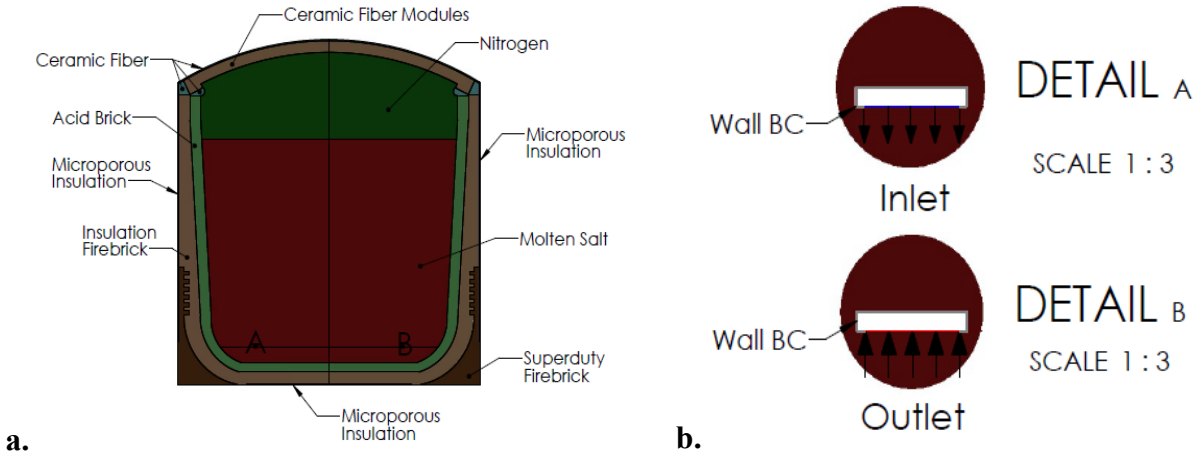

FIGURE 1. (a) 2D flow simulation model for circulating salt within a tank, and (b) Detailed view of inlet and outlet modelling geometries.

Error! Reference source not found. shows the mesh used in the simulation of the circular flow operation. The charging and discharging simulations use a similar meshing scheme as the mesh shown in **Error! Reference source not found.**. **Error! Reference source not found.** details the mesh size for the regions of the 2D tank geometry used in the circular, charging, and discharging models. The meshes for these models are comprised of quadratic elements via a pave meshing scheme.

TABLE 1. Meshing scheme for 2D circular flow, charging, and discharging models.

Geometry Region	Mesh Size
Molten Salt	2 cm, 2 mm refinement around inlet & outlet
Nitrogen	2 cm
Acid Brick	3 cm
Insulation Firebrick	3 cm
Superduty Firebrick	3 cm
Ceramic Fiber Modules	3 cm
Ceramic Fiber	3 cm & 1 cm on roof section
Microporous Insulation	1 cm

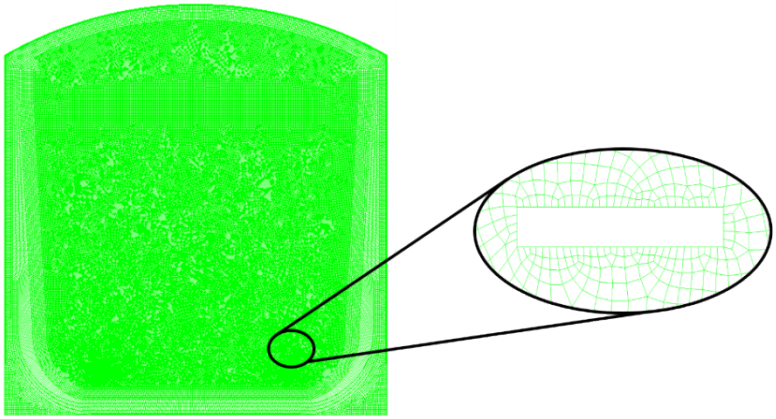

FIGURE 2. Mesh for circulating flow simulations with detail view around outlet area.

Flow, turbulence, and energy constitutive equations were solved for all operational phases of the two Gen 3 molten salt tanks. **Error! Reference source not found.** lists the primary model equations solved within all simulations for the thermal-fluid transient operation of the molten salt tanks. Eqns. (2), (3), and (4) are used to compute fluid flow by conserving mass and momentum. The thermal analysis used Eqn. (5) for fluids, and equation (6) for the solid walls which only account for conduction and convection. Turbulence was solved for with equations (7) and (8).

TABLE 2. Equations solved for all the simulations for the operation of the molten salt tanks.

Equation Formula	Number
$\frac{\partial \boldsymbol{\rho}}{\partial \boldsymbol{t}} + \nabla \cdot (\boldsymbol{\rho}\vec{\boldsymbol{v}}) = \boldsymbol{S_m}$	(2)
$\frac{\partial}{\partial \boldsymbol{t}}(\boldsymbol{\rho}\vec{\boldsymbol{v}}) + \nabla \cdot (\boldsymbol{\rho}\vec{\boldsymbol{v}}\vec{\boldsymbol{v}}) = -\nabla \boldsymbol{p} + \nabla \cdot (\bar{\bar{\boldsymbol{\tau}}}) + \boldsymbol{\rho}\vec{\boldsymbol{g}} + \vec{\boldsymbol{F}}$	(3)
$\bar{\bar{\boldsymbol{\tau}}} = \boldsymbol{\mu}\left[(\nabla\vec{\boldsymbol{v}} + \nabla\vec{\boldsymbol{v}}^{\boldsymbol{T}}) - \frac{\mathbf{2}}{\mathbf{3}}\nabla \cdot \vec{\boldsymbol{v}}\boldsymbol{I}\right]$	(4)
$\frac{\partial}{\partial \boldsymbol{t}}(\boldsymbol{\rho E}) + \nabla \cdot (\vec{\boldsymbol{v}}(\boldsymbol{\rho E} + \boldsymbol{p})) = \nabla \cdot \left(\boldsymbol{k_{eff}}\nabla \boldsymbol{T} - \sum_{\boldsymbol{j}} \boldsymbol{h_j}\vec{\boldsymbol{J_j}} + (\bar{\bar{\boldsymbol{\tau}}}_{\boldsymbol{eff}} \cdot \vec{\boldsymbol{v}})\right) + \boldsymbol{S_h}$	(5)
$\frac{\partial}{\partial \boldsymbol{t}}(\boldsymbol{\rho h}) + \nabla \cdot (\vec{\boldsymbol{v}}\boldsymbol{\rho h}) = \nabla \cdot (\boldsymbol{k}\nabla \boldsymbol{T}) + \boldsymbol{S_h}$	(6)
$\frac{\partial}{\partial \boldsymbol{t}}(\boldsymbol{\rho k_t}) + \frac{\partial}{\partial \boldsymbol{x_i}}(\boldsymbol{\rho k_t u_i}) = \frac{\partial}{\partial \boldsymbol{x_j}}\left[\left(\boldsymbol{\mu} + \frac{\boldsymbol{\mu_t}}{\boldsymbol{\sigma_k}}\right)\frac{\partial \boldsymbol{k_t}}{\partial \boldsymbol{x_j}}\right] + \boldsymbol{G_k} + \boldsymbol{G_b} - \boldsymbol{\rho\varepsilon} + \boldsymbol{Y_m} + \boldsymbol{S_k}$	(7)
$\frac{\partial}{\partial \boldsymbol{t}}(\boldsymbol{\rho\varepsilon}) + \frac{\partial}{\partial \boldsymbol{x_i}}(\boldsymbol{\rho\varepsilon u_i}) = \frac{\partial}{\partial \boldsymbol{x_j}}\left[\left(\boldsymbol{\mu} + \frac{\boldsymbol{\mu_t}}{\boldsymbol{\sigma_\varepsilon}}\right)\frac{\partial \boldsymbol{\varepsilon}}{\partial \boldsymbol{x_j}}\right] + \boldsymbol{C_{1\varepsilon}}\frac{\boldsymbol{\varepsilon}}{\boldsymbol{k_t}}(\boldsymbol{G_k} + \boldsymbol{C_{3\varepsilon}G_b}) - \boldsymbol{C_{2\varepsilon}\rho}\frac{\boldsymbol{\varepsilon^2}}{\boldsymbol{k_t}} + \boldsymbol{S}_{\boldsymbol{\varepsilon}}$	(8)

The design of salt piping inlet and outlet ports was altered from the tank's true design due to the two-dimensional nature of the model. Modeling the tanks in two dimensions with flow pipes which transverse the height of the tanks would restrict flow in the tank. This flow restriction would in turn be unrealistic as the molten salt within the tank would be easily by able flow around the inlet and outlet piping. To better represent the 3D flow in two dimensions, two small, 1 cm, portions of the piping were created in the model to flow the molten salt in and out of the tank. These small portions of the piping contain either an inlet or outlet the size of the inner diameter of the pipe surrounded by wall-type boundary conditions the size of the wall thickness of the pipe. The boundary conditions for the model are shown in Table 3. In particulat, the wall-type boundary conditions surrounding the inlet and outlet were needed for convergence of the flow. The solver preforms better when the flow is perpendicular to the inlet and outlet, which the walls help directing the flow to be perpendicular to the surface of the inlet and outlet. If the model did not have the walls surrounding the inlet and outlet the solver would predict flow reversal and lead to unstable convergence behavior causing unreliable and unrealistic results. The molten salt is at the maximum normal operating level with the rest of the tank's head space cavity filled with nitrogen gas ullage gas. Various layers of different solid materials surround the molten salt and nitrogen regions in the model.

TABLE 3. Boundary conditions for circular flow CFD modeling.

Boundary Conditions	Value
Molten Salt Inlet Velocity	1.56 m/s (47 GPM) & 3.64 m/s (110 GPM)
Molten Salt Outlet Pressure	0 Pa
Molten Salt Inlet Temperature	500 °C & 720 °C
Tank Body External Wall Convection	5 W/m^2-K at 30 °C

All the interfaces between different materials in the model were modeled as coupled walls which matches the temperature of the materials in contact at the interface but does not allow flow through the interface. This model allowed for a two-dimensional simulation of circular flow in the molten salt tanks in good approximation of the 3D

flow as most of the tank contains a continuous domain of molten salt. **Error! Reference source not found.** details the boundary conditions used in the CFD analysis of the circular flow operation of the molten salt tanks.

RESULTS & DISCUSSION

Steady Analysis

Simulations of the circulating flow phase where performed for both cold and hot tanks at 500 °C and 720 °C respectively. These are the predefined operating temperatures for the Gen 3 Liquid-Pathway pilot-scale system. Both tank temperatures were simulated at predetermined engineered flow rates of 47 GPM and 110 GPM. These were predetermined flow rates for the 2.0 MW_{th} system by Sandia for the pilot-scale system [17]. All external walls for these simulations were set to have a convection boundary condition of 5 W/m^2-K at 30 °C based on the Churchill and Chu correlation for free convection [18]. The results of the circulating flow simulations are shown in **Error! Reference source not found.** for a spacing of 3.85 m between the intel and outlet of the flow loop.

TABLE 4. Temperatures of circulating flow simulations for 3.85 m flow loop spacing.

Modeled Case	Average Salt Temperature	Minimum Salt Temperature	Average N_2 Temperature	Minimum N_2 Temperature
Cold Tank at 47 GPM	499.83 °C	499.98 °C	498.86 °C	495.74°C
Cold Tank at 110 GPM	499.90 °C	499.99 °C	498.94 °C	495.93 °C
Hot Tank at 47 GPM	719.65 °C	719.98 °C	719.42 °C	715.97 °C
Hot Tank at 110 GPM	719.98 °C	719.78 °C	718.92 °C	716.10 °C

The ports spacing was optimized within the tank, and produced minimal thermal gradients within both the molten salt and nitrogen gas head space. The higher flow rate resulted in smaller thermal gradients than the slower flow rates as the molten salt mixes better (an increase of around 120% in the heat transfer coefficient) at the higher velocities associated with the higher flow rate. The spacing of 3.85 m was the initial value tested and resulted in a highly uniform temperature distribution. This temperature distribution was classified as sufficient for the operation of the tanks as it minimized thermal gradients across the fluid media. **Error! Reference source not found.** and **Error! Reference source not found.** show the temperature distributions and velocity vector fields for the cold and hot tank respectively at 47 GPM. The thermal gradients within the molten salt are greater for the 47 GPM flow rate and is the reason the temperature distribution for these cases are shown below. From these figures, the minimum overall temperature in the molten salt domain occurred at the regions with the lowest flow. The approximations used in this model likely underestimate the thermal gradients in the molten salt medium as the flow will likely be more obstructed due to piping and three-dimensional effects in reality. This was not captured in this model. In the actual operation of the tanks, a flow loop spacing (the distance from the center of the outlet to the center of the inlet) of 3.85 m will likely provide minimal thermal gradients within the molten salt during circular flow operation.

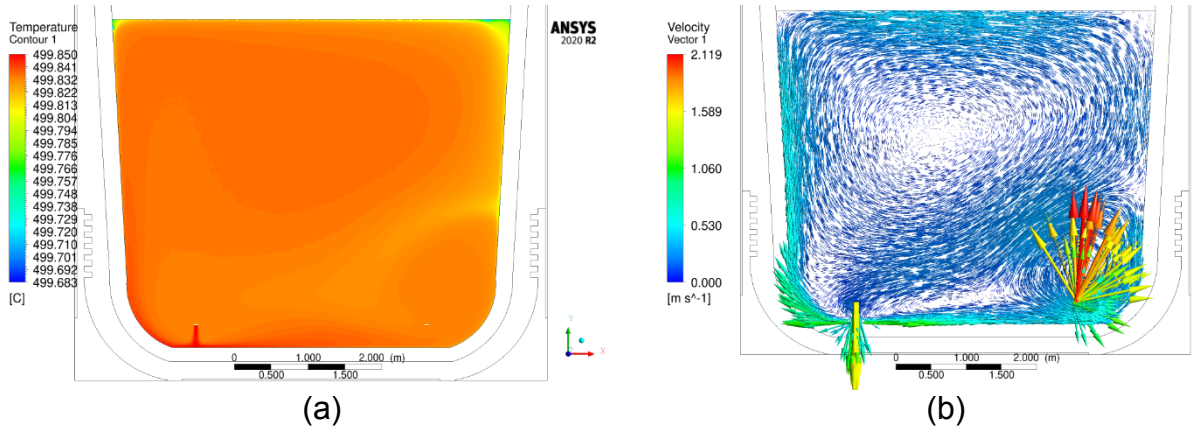

FIGURE 3. (a) Molten salt temperature distribution, and (b) Velocity vector field for cold tank salt circulation at 47 GPM.

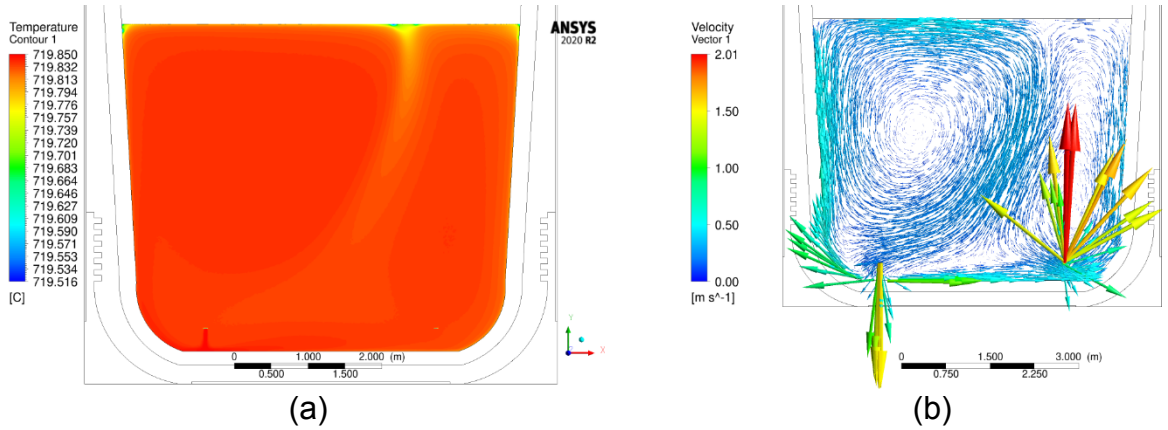

FIGURE 4. (a) Molten salt thermal distribution, and (b) Velocity vector field for hot tank salt circulation at 47 GPM.

Transient Analysis

The charging operation of the hot molten salt tank was simulated to investigate the thermal gradients which developed over the transient period investigated. The main source of mechanical stress on the tank body is due to nonuniform thermal expansion caused by large temperature gradients. **Error! Reference source not found.** shows the temperature of the molten salt, nitrogen ullage gas, and acid brick (the layer under the most thermal stress) during the charging of the hot molten salt tank. The molten salt volume fraction and velocity vector fields of the molten salt and nitrogen are shown in **Error! Reference source not found.** and **Error! Reference source not found.** respectively. The largest thermal gradients during the charging phase is on the left side of the tank near the inlet between the molten salt and the acid brick. This area of the tank experiences the largest thermal gradients due to the higher-temperature molten salt rising from the inlet, and the nitrogen advecting heat from the right to the left of the tank. The flow of the nitrogen becomes steady after approximately 10 minutes and the molten salt flow increases slowly as the overall molten salt level rose. The side of the acid brick nearest to the inlet of the tank has the highest risk of experiencing high thermal stress.

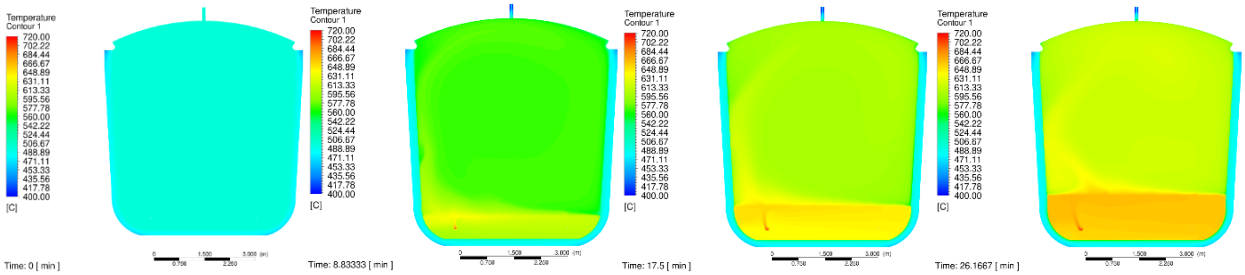

FIGURE 5. Temperature of molten salt, nitrogen, and acid brick during the charging of the hot tank.

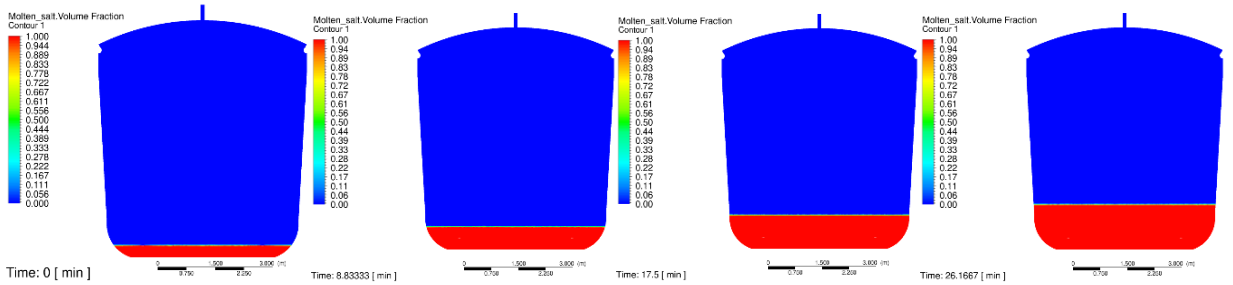

FIGURE 6. Molten salt volume fraction during the charging of the hot tank.

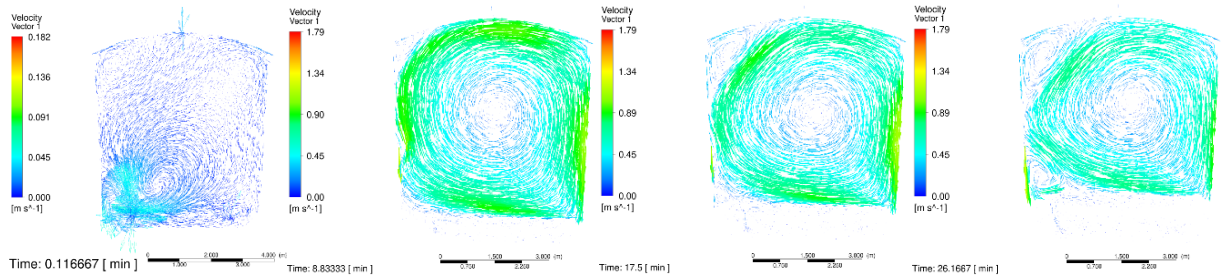

FIGURE 7. Velocity vector fields of molten salt and nitrogen during the charging of the hot tank.

CONCLUSION

A steady and transient circulating flow model was developed for cold and hot tanks, considered for a 1 MWth CSP pilot-plant, operating at 500°C and 720°C respectively. Preliminary results suggest that higher flow rates result in smaller thermal gradients (<2°C overall) than with lower flow rates as the molten salt mixes at higher velocities associated with the higher flow rate for the particular tank storage geometry. Overall thermal gradients for the steady flow model are shown to be less 1°C with overall circulation velocities as high as approximately 2.1 m/s. For steady operation, the spacing ports had minimal thermal gradients within both the molten salt and nitrogen gas control volumes. Higher flow rates of salt passing into and out of the tanks resulted in smaller thermal gradients than the slower flow rates as the molten salt mixes better (an increase of around 120% in the heat transfer coefficient) at the higher velocities associated with the higher flow rate. The port spacing of 3.85 m was found to have a highly uniform temperature distribution. This temperature distribution was classified as sufficient for the operation of the tanks as it minimized thermal gradients across the fluid media. For the unsteady model, the flow of the nitrogen was found to become steady after approximately 10 minutes and the molten salt flow was found to increase slowly as the overall molten salt level rose.

ACKNOWLEDGMENTS

Sandia National Laboratories is a multimission laboratory managed and operated by National Technology and Engineering Solutions of Sandia, LLC., a wholly owned subsidiary of Honeywell International, Inc., for the U.S. Department of Energy's National Nuclear Security Administration under contract DE-NA0003525.

REFERENCES

(Use the Microsoft Word template style: *Heading 1*) or (Use Times New Roman Font: 12 pt, Bold, ALL CAPS, Centered)

References should be numbered using Arabic numerals followed by a period (.) as shown below and should follow the format in the below examples.

1. Rodríguez, I., Pérez-Segarra, C.D., Lehmkuhl, O. and Oliva, A., 2013. Modular object-oriented methodology for the resolution of molten salt storage tanks for CSP plants. Applied Energy, 109, pp.402-414.
2. Mehos, M., Turchi, C., Vidal, J., Wagner, M., Ma, Z., Ho, C., Kolb, W., Andraka, C. and Kruizenga, A., 2017. Concentrating solar power Gen3 demonstration roadmap (No. NREL/TP-5500-67464). National Renewable Energy Lab.(NREL), Golden, CO (United States).
3. Bonk, A., Sau, S., Uranga, N., Hernaiz, M. and Bauer, T., 2018. Advanced heat transfer fluids for direct molten salt line-focusing CSP plants. Progress in Energy and Combustion Science, 67, pp.69-87.
4. Fernández, A.G., Gomez-Vidal, J., Oró, E., Kruizenga, A., Solé, A. and Cabeza, L.F., 2019. Mainstreaming commercial CSP systems: A technology review. Renewable energy, 140, pp.152-176.
5. Zurigat Y, Maloney K, Ghajar A. A comparison study of one-dimensional models for stratified thermal storage tanks. J Solar Energy Eng 1988; 111:204–10.

6. Alizadeh S. An experimental and numerical study of thermal stratification in a horizontal cylindrical solar storage tank. Solar Energy 1999;66(6):409–21.
7. Ghaja AJ, Zurigat YH. Numerical study of the effect of inlet geometry on stratification in thermal energy storage. Numer Heat Transfer, Part A 1991;19:65–83.
8. Kleinbach E, Beckman W, Klein S. Performance study of one-dimensional models for stratified thermal storage tanks. Solar Energy 1993;50(2):155–66.
9. Gabbrielli R, Zamparelli C. Optimal design of a molten salt thermal storage tank for parabolic trough solar power plants. J Solar Energy Eng 2009;131(4).
10. Papanicolaou E, Belessiotis V. Transient natural convection in a cylindrical enclosure at high Rayleigh numbers. Int J Heat Mass Transfer 2002;45:1425–44.
11. Oliveski RDC, Krezinger A, Vielmo H. Cooling of cylindrical vertical tanks submitted to natural internal convection. Int J Heat Mass Transfer 2003;46:2015–26.
12. Rodriguez I, Castro J, Pèrez-Segarra C, Oliva A. Unsteady numerical simulation of the cooling process of vertical storage tanks under laminar natural convection. Int J Therm Sci 2009;48(4):708–21.
13. Flueckiger S, Yang Z, Garimella SV. An integrated thermal and mechanical investigation of molten-salt thermocline energy storage. Appl Energy 2011;88(6):2098–105.
14. Xu C, Wang Z, He Y, Li X, Bai F. Sensitivity analysis of the numerical study on the thermal performance of a packed-bed molten salt thermocline thermal storage system. Appl Energy 2012;92:65–75.
15. Gandhi, M.S., Joshi, J.B., Nayak, A.K., Vijayan, P.K., 2013. Reduction in thermal stratification in two phase natural convection in rectangular tanks: {CFD} simulations and {PIV} measurements. Chem. Eng. Sci. 100, 300–325, 11th International Conference on Gas-Liquid and Gas-Liquid-Solid Reactor Engineering.
16. L.F. Handy-Cardenas, K.M. Armijo, M.D. Carlson, M. Anderson, and A. Overacker, "Modelling of select operational modes of a 2.0MWth sodium/molten pilot system/CSP Gen 3 Liquid Phase Design," 2021 SolarPACES Conference, Albuquerque, NM, USA, (2021).
17. Armijo, K.M., Carlson, M.D., Dorsey, D.S., Christian, J.M. and Turchi, C.S., 2020, June. System Design of a 2.0 MWth Sodium/Molten Salt Pilot System. In Energy Sustainability (Vol. 83631, p. V001T02A004). American Society of Mechanical Engineers.
18. S. W. Churchill and H. H. Chu, International Journal of Heat and Mass Transfer, pp. 1323-1329, 1975.M. P. Brown and K. Austin, Appl. Phys. Letters 85, 2503–2504 (2004).
19. Rivas, E., Rojas, E., Bayón, R., Gaggioli, W., Rinaldi, L. and Fabrizi, F., 2014. CFD model of a molten salt tank with integrated steam generator. Energy Procedia, 49, pp.956-964.